2019

ESTABLISHMENT AND CHARACTERIZATION OF ERASTIN-RESISTANT TRIPLE NEGATIVE BREAST CANCER CELL MODELS

Morgan Charbonneau
Michigan Technological University, mlcharbo@mtu.edu

ESTABLISHMENT AND CHARACTERIZATION OF ERASTIN-RESISTANT TRIPLE NEGATIVE BREAST CANCER CELL MODELS

By

Morgan Charbonneau

A THESIS

Submitted in partial fulfillment of the requirements for the degree of

MASTER OF SCIENCE

In Biological Sciences

MICHIGAN TECHNOLOGICAL UNIVERSITY

2019

This thesis has been approved in partial fulfillment of the requirements for the Degree of MASTER OF SCIENCE in Biological Sciences.

Department of Biological Sciences

Thesis Advisor:	*Xiaohu Tang*
Committee Member:	*Ebenzer Tumban*
Committee Member:	*Thomas Werner*
Department Chair:	*Chandrashekhar Joshi*

Table of Contents

Acknowledgements

I would like to thank Dr. Xiaohu (Mark) Tang for all of the help with analyzing data and planning experiments. Additionally, thank you to Tahiyat Alothaim for always answering my plethora of questions, training me of various assays, and willingness to help in all aspects. A special thanks to my department for funding throughout this degree. Finally, thank you to my committee members, Dr. Ebenezer Tumban and Dr. Thomas Werner, for their willingness to serve on my committee and making this degree possible.

List of abbreviations

TNBC: Triple-negative breast cancer

MDA231 E^R: MDA231 cell line resistant to Erastin

MDA231 C^R: MDA231 cell line resistant to cysteine deprivation

BT549 E^R: BT549 cell line resistant to Erastin

HBL100 E^R: HBL100 cell line resistant to Erastin

Abstract

Breast cancer is a collection of heterogeneous diseases and the most common cancer in females worldwide. Breast cancer is often categorized by the distinctive expression of membrane biomarkers including estrogen receptor (ER), progesterone receptor (PR), and human epidermal growth factor receptor-2 (Her2). Breast cancer has four main subtypes: luminal A, luminal B, basal-like, and HER2-positive. Of all breast cancer types, triple-negative breast cancer (TNBC) is the most aggressive metastatic subtype, accounting for 15~20% with the basal-like and claudin-low features, and lack of effective targeted therapies due to the absence of cell membrane receptors. In recent research, metabolic dysregulation has been noted as a hallmark of cancer, which can be used to design targeted therapies specific for a certain metabolic weakness of cancer. Cystine, the oxidized dimer of cysteine, is transported into the cell and a major source of glutathione (GSH), which maintains the cellular redox balance. Mesenchymal TNBC has been found to be cysteine-addictive/dependent and requires excess cystine to survive. Although limiting cellular cystine/cysteine is an efficient strategy to kill most of TNBC tumor cells, we observed that a portion of tumor cells remains to survive and expand after cellular cysteine depletion by erastin, an inhibitor of cystine transporter. This *in vitro* observation may substantially mimic tumor relapse in patients after targeted cysteine-addiction therapy. The three aims of this study are: 1) Develop *in vitro* erastin-resistant TNBC cell models; 2) Understand the underlying mechanisms of erastin-resistance; and 3) Identify potential sensitizers to overcome the erastin-resistance in tumor cells. First, we established three erastin-resistant cell systems derived from cystine-addictive TNBCs.

Second, we identified potential combinative sensitizers to eradicate the erastin-resistant tumor cells by an epigenetic compound library screen approach. Last, we performed microarray gene expression profiling analysis and found distinct gene expression patterns between erastin-resistant and erastin-sensitive cells that will help uncover the underlying mechanism of erastin-resistance. Identification of combinative sensitizers and understanding the erastin resistance may help designing an optimal therapeutic strategy to prevent tumor recurrence in patients.

Chapter 1:

1.1 Introduction

1.1.2 Breast cancer is a collection of heterogeneous diseases with various subtypes

There is an estimated 18.1 million new cases of cancer in 2018[1]. For both sexes, breast and lung cancers are tied for the highest number of incidences at around 2.1 million each [1]. Breast cancer is commonly classified by three main strategies: morphological (ductal, lobular, etc.), receptors (estrogen, progesterone, etc.), and intrinsic subtype (basal-like, luminal, etc.) [2, 3]. From these criteria, there are five main subtypes of breast cancer including Luminal A, Luminal B, claudin-low, Basal, and HER2-overexpression, as well as a normal-like breast cancer [2, 4-7]. Of all subtypes, the majority of deaths occur from triple-negative breast cancer (TNBC) which makes up 60-82% of all basal-like breast cancers [4, 5, 7]. TNBC is also of the claudin-low subtype, but it is less common [7]. TNBC is characterized by its lack of progesterone and estrogen receptors (ER-/PR-) as well as the lack of over-expression of human epidermal growth factor receptor 2 (HER2-) [4, 7]. Of the 2.1 million new breast cancer cases each year, 10-15% are expected to be of the triple-negative breast cancer genotype [1, 4, 8]. This form of cancer is more common in young African American and Hispanic women, who are under the age of 50 [1, 4, 8].

Although there is no consensus on the cause of TNBC, a nonhereditary breast cancer type 1 (BRCA1) mutation is suggested as the most common cause by microarray

and immunohistochemical studies [4, 9]. Additionally, for all BRCA1 mutation breast cancers, TNBC or basal-like subtypes make up 75% of those diagnosed which supports this suggestion [4, 7]. Along with the BRCA1 mutation, TNBCs commonly lack retinoblastoma protein (Rb) and p53 proteins allowing them to proliferate at quicker rates [7]. For TNBC tumors that are not of the basal-like subtype, but that are instead claudin-low, they are found to be enriched with properties similar to breast stem cells and epithelial-to-mesenchymal transition [4, 10]. Claudin-low cancers have a better prognosis than basal-like, but only make up less than 20% of TNBCs [4, 5].

1.1.3 Cancer metabolism dysregulation as a hallmark of cancer

Cancer cells have been found to acquire six biological capabilities along with two new potential capabilities and two enabling characteristics [11, 12]. The six that were first discovered and have been known for nearly two decades include sustaining proliferative signaling, resisting cell death, inducing angiogenesis, enabling replicative immortality, activating invasive metastasis, and evading growth suppressors [11]. More recently, two enabling characteristics have been identified, which are genome instability and mutation, and tumor-promoting inflammation [12]. Along with the characteristics, new capabilities, such as evading immune destruction and deregulating cellular energetics, have been suggested as emerging hallmarks and have become the focus of cancer research [12].

Deregulation of cellular energetics has been seen in cancer cells for decades. It was primarily known as the Warburg Effect, where cancer cells breakdown their glucose

to lactate regardless of oxygen availability [13, 14], whereas a healthy somatic cell would breakdown their glucose into pyruvate and oxidize the products to CO_2 through glycolysis and the tricarboxylic acid cycle (TCA cycle) [14]. It was also thought that the Warburg Effect was due to mitochondrial defects that inhibited cancer cells' ability to breakdown the glucose into CO_2 [13-15]. Recently, the idea of mitochondrial defects has been proven incorrect. The mitochondria in cancer cells are actually not defective, but are rather reprogrammed in proliferating cells for macro-molecular synthesis [14].

There is now evidence to support the idea that the main role of activated oncogenes and inactivated tumor suppressors is to reprogram a cell's metabolism [14]. An example of these oncogenes is the transcription factor Myc, which is known to promote glutaminase expression [14, 16]. This enzyme, when impaired in oncogenic cells, leads to apoptosis, which further shows the connection between oncogenes and a transformed metabolism [14, 16, 17].

In addition to oncogene activation, the deactivation of tumor suppressors leads to a change in metabolism. When tumor suppressor p53 is activated, it is dire for the cells as they are pushed to undergo apoptosis in a glucose-deprived environment [14]. However, when p53 is inactive in tumors, it has been shown to increase anabolic synthesis of macromolecules from glycolytic intermediates [14, 15]. This is just one example of how inactivation of tumor suppressors can benefit the reprogramming of a cancer cell's metabolism. This new information shows how cancer cell metabolism is actively reprogrammed by oncogenes and tumor suppressors and explains how cancer metabolism dysregulation is a hallmark of cancer.

1.1.4 Targeting metabolic vulnerability as an important and precise strategy to eradicate cancer

The ability to study cancer cell metabolism has greatly increased research into targeted therapies. When cancer cells change their metabolism, such as the Warburg Effect, they differ from normal tissue cells. The cells require metabolites, like excess glucose, that a quiescent cell does not [2, 18]. This behavior creates specific targets that would cause less adverse side effects to patients when treated. Metabolomics has found potential biomarkers for diagnosis, disease progression, and oncometabolites [2, 19]. Today, clinical treatments include antipurines, antipyrimidines, and antifolates for a broad spectrum of cancers [2, 18, 20]. Most cancers have a higher nutrient intake requirement which leads to these therapeutic targets.

However, specific treatments are needed to reduce adverse side effects and improve outcomes. It is suspected that each molecular subtype of cancer has a different metabolic phenotype [2, 6, 13, 20]. Specifically, breast cancer subtypes have distinct metabolite differences that can be targeted for precise treatment. These treatments include anti-Estrogen for ER+ cancers and anti-HER2 for HER2+ cancers. However, for cancers that lack these common receptors, such as TNBC, these treatments are ineffective [2, 6, 21]. Knowing the subtype of cancer is important in order to provide specific treatment that will target the precise metabolic vulnerability.

Receptors, such as ER an HER2, are just one example of a metabolic target. Other alterations in the metabolism can also be targeted by specific treatments. Other targets

include upregulated pathways, such as glycolysis, the TCA cycle, and lipid metabolism [2, 14, 18]. Through the use of labeled metabolites, researchers have been able to determine intracellular metabolic targets with magnetic resonance spectroscopy (MRS). With this process, a newly discovered metabolic proto-oncogene, isocitrate dehydrogenase (IDH), has been found to have mutations in two of its entities: IDH1 and IDH2 [16, 19]. These mutations have been linked to glutamine nutrient requirement in cancer cells. Targeting these enzymes doesn't affect normal cell metabolism as harshly [19].

Another main target is nucleotides [2, 4, 16, 21]. Targeting nucleotides affects all rapidly proliferating cells by stopping their DNA and RNA production [2, 18, 19]. This form of treatment causes adverse side effects on the patient because as normal cells are also targeted. This is the reason why more recent studies started targeting amino acid addiction instead. A nutrigenetic screen can be done to determine to which, if any, amino acids a subtype is addicted [16]. The lack of these specific amino acids in the surrounding environment would then cause programmed cell death. By targeting metabolic vulnerabilities of each specific molecular subtype, their amino acid addictions, and metabolic phenotypes, a new plethora of targeted therapies can be developed that are specific for the molecular subtypes of cancer, even precisely for each individual patient.

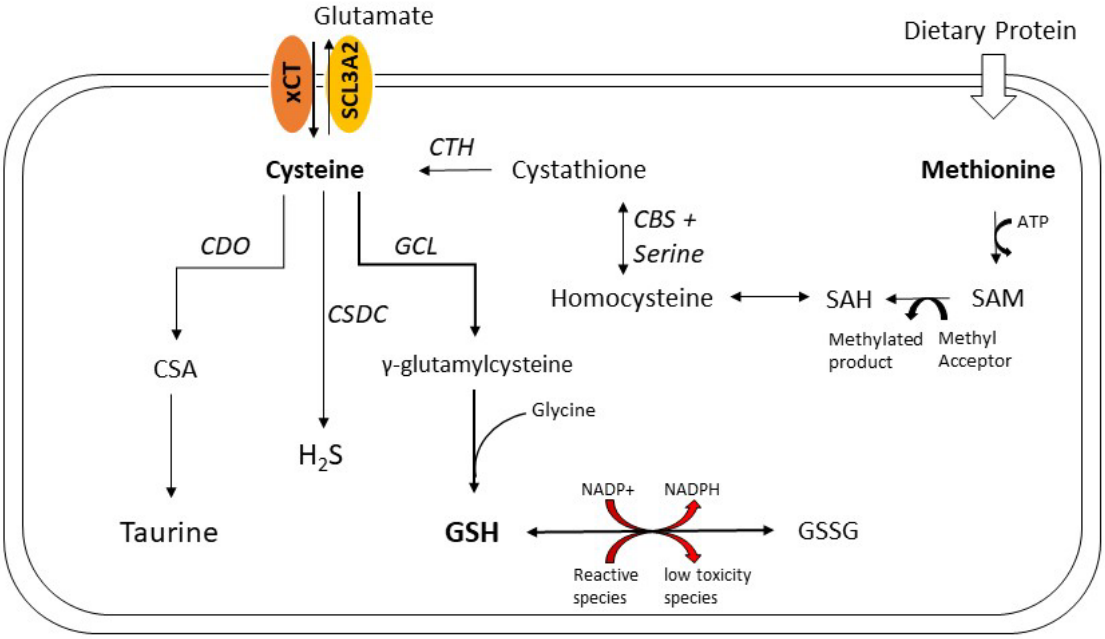

Figure 1: Illustration of cellular cysteine metabolism. Metabolic pathways of cyst(e)ine beginning from SCL7A11 antiporter or methionine. When brought into the cell as methionine, the molecule converts to SAM through the use of ATP. This product is then converted to SAH by de-methylation and an S_N2 reaction creates a product known as homocysteine. Homocysteine undergoes a condensation reaction to form cystathione which forms cysteine aided by CTH. If cystine enters the cell through the xCT antiporter; the double molecule can be split to form cysteine. This amino acid then continues down the necessary pathway to form taurine, sulfate (H_2S), or glutathione (GSH).

1.1.5 Cysteine metabolism and functions in cancer

Cysteine is an unstable amino acid in which two cysteine molecules join by a disulfide bond in order to form a more stable version known as cystine. Cysteine is consumed and produced through a multitude of different pathways. There are two major routes to supply cellular cysteine (**Figure 1**). One is that cysteine is formed from methionine via cellular cysteine biosynthesis. The other route is that cystine is brought into the cell through the cystine transporter (xCT) and reduced to cysteine. Besides as building blocks of protein synthesis, cysteine is used to synthesize sulfate, taurine, or glutathione (GSH) [20-23]. Methionine undergoes a methyl transfer to S-Adenosyl

methionine (SAM) aided by ATP. This byproduct is then converted into S-Adenosyl homocysteine (SAH) through a S_N2 mechanism that leaves homocysteine [24]. Cystathionine β-synthase catalyzes a condensation reaction, where homocysteine combines with serine and becomes cystathionine. Cystathionine γ-lyase then aids in the conversion of cystathionine to cysteine and two byproducts [24].

Besides being a building block of protein synthesis, cysteine is used ot synthesize sulfate, taurine, and glutathione (GSH) [20, 21, 23, 24]. Which metabolite is synthesized from cysteine has been found to be determined by the concentration of cysteine [21, 25]. At high concentrations, sulfate and taurine are favored, while at low concentrations, GSH is favored [21]. GSH acts as a storage unit for cysteine and can be broken down to release the amino acid when needed. GSH breakdown is completed in individual cells, but in larger scale by the liver of humans. The amount of cysteine available is regulated by cysteine deoxygenase (CDO), glutamate-cysteine ligase (GCL), and cysteine-sulfinate decarboxylase (CSDC) (Figure 1) [21, 25]. CDO adds a sulfonate group to cysteine to form cysteine sulfinic acid (CSA), which can then be further transformed into taurine. CSDC removes a pyruvate group and an NH_3 group in the process of forming H_2S.

GCS and GSH synthases catalyze the reaction to form GSH from cysteine in a two-step reaction [17, 21, 26]. γ-glutamylcysteine is formed from cysteine and glutamate with the help of ATP and glutamate cysteine ligase (GCL) [17, 26]. GCL is made of two subunits: the catalytic subunit (GCLC) and the modifier subunit (GCLM). After the first step, γ-glutamylcysteine is converted to GSH by GSH synthetase and the addition of glycine [20, 21, 26]. This step also requires ATP.

The production of GSH is arguably the most important function of cysteine metabolism. GSH has antioxidative effects by acting as a substrate to molecules that turn reactive oxygen species (ROS) into less harmful materials, such as fatty acids [27, 28]. When GSH is oxidized by glutathione peroxidase (GPx), it becomes known as GSSG [26, 27]. In this form, tissues are protected from the side effects of peroxidation, but it doesn't perform the same functions as GSH [26, 27]. GSH or its derivatives activate multiple signaling molecules that are necessary for proliferation, morphogenesis, and differentiation [27]. In cancer, both of these functions lead to a higher viability.

1.1.6 Targeting cysteine vulnerability to eradicate TNBC

Basal-like TNBC has been found to be addicted to cystine through a nutrigenetic screen, while luminal-type cancers and normal cells were found to be cystine-independent [16]. This creates a potential target that is specific to TNBC tumors. Cysteine metabolism begins with cystine, two cysteine molecules connected by a disulfide bond, being transported into the cell through the xCT transporter [2, 16, 20, 25]. xCT, formed by the gene SCL7A11, is upregulated in cancers due to oxidative stress [22]. The antiporter is heterodimeric, where xCT is the light subunit and CD98 is the heavy subunit [22]. This antiporter functions to take cystine into the cell while releasing glutamate. Since cysteine is required to form GSH, targeting this particular amino acid would halt the production and force the cancer cells to undergo programmed cell death. Targeting this altered metabolic state that is specific to TNBC could be a promising potential target.

1.1.7 Drug resistance and cancer recurrence are current therapeutic challenges

Currently, cancer treatments include chemotherapy, radiation, surgery, and in a few cases, hormone therapy. TNBC patients cannot benefit from the new hormone therapies, such as anti-HER2 drugs, since they lack the receptors these treatments target. For these tumors, the general course of treatment is chemotherapy with common cytotoxic drugs, surgery, followed by radiation [3]. The main classes of chemotherapy drugs include anthracyclines and taxanes, and the tumors have shown a promising response for most patients [3]. While the tumors may respond to this treatment, the reoccurrence rate of TNBC is much higher in the first three to four years than it is for other breast cancers [3, 5, 29]. When these new tumors grow, they are often resistant to the chemotherapeutic drugs that were used during the first round and more aggressive [30, 31]. How to predict the recurrence of tumors is still unknown, but general factors have been found to be associated with recurrence. These factors include histological grade, lymph node status, tumor size [32-34], and the presence or absence of hormone receptors including progesterone (ER), estrogen (PR), and human epidermal growth factor receptor 2 (HER2) [35]. Overcoming this resistance in a clinical setting entails the use of neoadjuvant therapy and creating a concoction of cytotoxic drugs [3, 4]. Further research is attempting to determine these resistant pathways and target the genes responsible.

As stated previously, TNBC commonly reoccurs in patients. Previous studies have found TNBC to be cyst(e)ine-dependent, and the majority of cells underwent

necrosis in the presence of a cystine transport inhibitor (erastin) or in the absence of cysteine [16]. A small portion of cells was found to survive these treatments and potentially mimic recurrent TNBC tumors [16].

The aims and objectives of this thesis were as follows:

i. Develop *in vitro* erastin-resistant TNBC models. Although some TNBCs are cysteine-addictive and highly sensitive to cysteine depletion, we found that a portion of addictive TNBC cells is able to survive and expand after blocking cystine transport by the inhibitor of cystine antiporter erastin. This survival might mimic recurrent TNBC tumors *in vivo* after targeted cysteine addiction therapy. The successful establishment of an *in vitro* erastin-resistant model will allow for further study on the mechanisms of drug resistance and optimize therapeutic regimen.

ii. Identify potential sensitizers of erastin-resistance to overcome the erastin-resistance in tumor cells. The combination therapy with sensitizers would overcome the erastin resistanc and prevent tumor recurrence in patients. Potential sensistizers will be indentified by an epigenetic compound library screen approach.

iii. Understand the underlying mechanisms of erastin-resistance. The gene expression profile in erastin-resistant and –sensitive TNBCs will be analyzed by expression of microarray analysis to explore the resistance mechanism. Treatment and prevention can be further optimized based on the understanding of the mechanisms of drug resistance.

1.2 Methods

1.2.1 Cell Culture (Sensitive to resistant, infections)

All human tumor cells in this study were cultured in Dulbecco's modified eagle's medium (DMEM, Hyclone) supplemented with 10% fetal bovine serum (FBS) and 1% of antibiotics (Penicillin/Streptomycin, Gibco) throughout the duration of the experiments. Cultures were kept in a humidified incubator at 37ºC and 5% CO_2. Cells were plated in 100 mm dishes for maintenance and split using 0.5% trypsin (Gibco) when needed. Amino acid-deficient medium was prepared from the powder of DMEM without any amino acids (Fisher Scientific). For cystine-deficient medium, all other amino acids (Sigma), except cystine, were added back according to the standard recipe of DMEM formulation.

1.2.1.1 *In vitro* resistance model establishment

To establish the cystine-insensitive cell models, three triple-negative breast cancer (TNBC) cell lines, MDA231, HBL100, and BT549, were used. MDA-MB-231 cells originated from an epithelial adenocarcinoma while BT549 were harvested from an invasive ductal carcinoma and HBL100 were derived from human lactation. Cells were treated with a low concentration of erastin for three days, after which surviving cells were collected and allowed to divide (**fig. 2**). This was repeated three times, then a higher concentration was used until 10 μM Erastin resistance was obtained.

1.2.2 Cell Survival and Death Assays

Cells were plated in 12-well plates typically in a concentration of $7x10^4$ cells per well and allowed for two days growth. Then the cells were treated as desired in triplicates. The Cytox Fluor™ Cytotoxicity Assay (Promega, Madison, WI, USA) was performed according to the company's protocol. The Cytotox Fluor™ Cytotoxicity Assay measures protease release of the cells and therefore necrosis. Briefly, once the treatments reached the indicated time points or cells showed 20-30% s cell death under a brightfield microscope, 25 µL medium from each well was placed in a 96-well white plate along with three wells of 25 µL prepared medium as assay references. The same volume (25 µL) of the Cytox Fluor™ Cytotoxicity Assay reagent was further added into each well, and the assay plate was incubated for 30 minutes at 37 ºC. The assay plate was read in a BioTek Synergy HTX fluorescence plate reader with a Green Filter cube at 485 nm excitation and 520 nm emission. The results were imported to Microsoft Excel 2016 or GraphPad Prism9 for data analysis. Statistical analysis such as standard deviation, error percentage, and significance were calculated. The 12-well plates were under further treatment and detected by a crystal violet (CV) staining assay to determine cell survival. At the indicated time, the medium was sucked out and replaced with 1 mL of crystal violet (CV) stain per well and uncubated overnight. The CV stain was removed and the wells were washed thoroughly and left to dry. The density of cell staining represents relative cell survival.

Alternatively, cell survival was measured by CellTiter-Glo Assay (Promega) that detect cellular ATP levels. The assay was performed in a clear 96-well plate at desired

cell numbers (typically 5000 cells per well). After two days, the cells were treated in quadruplet with desired treatments. At desired end time points, the plate was balanced at room temperature for 30 minutes. Then, 10 μL of CellTiter-Glo reagent was pipetted into each well including reference wells with only culture medium. The luminescence of the plate was read with BioTek Synergy HTX at a 160 gain value. The data were exported to Microsoft Excel 2016 or GraphPad Prism9 for further analysis.

1.2.3 Epigenetic Compound Library Screening

The desired cells were collected using Trypsin from a 100 mm maintenance plate. The control and Erastin plates were prepared using a multichannel pipette to move 3 μL of drugs from each well of the plate to a new, clear 96-well plate. A concentration of 5000 cells per well was prepared in DMEM ++ medium and 97 μL of medium and cells were added to each well for the control. The same procedure was followed for the Erastin plate, but a 5 μM concentration of erastin was added to the cell and medium mixture before plating. The plates were checked with a brightfield microscope daily, and differences in cell death between the control and Erastin plates were noted. After 72 hours, the plates underwent an ATP assay, as explained above. The results were exported and analyzed in Microsoft Excel 2016 or GraphPad Prism9.

1.2.4 Western Blot

Western Blot to determine various protein levels was completed similarly to previously published methods [16]. Cells were collected from 6-well plates. Cells were

lysed in RIPA buffer from Sigma, protease inhibitor, and PhosSTOP phosphatase inhibitor cocktail (Roche)[16]. The tubes were then vortexed and placed on ice. The Eppendorfs were then vortexed again and placed in a 4 ºC pre-cooled centrifuge at 13000 rpm for 15 minutes. The supernatant was transferred to newly labeled tubes without disturbing the pellet. The BCA assay was used to determine protein concentrations. A standard curve was created using 0.5 µg/mL and 2 µg/mL BSA stocks in a clear 96-well plate. The plate was placed in a 40 ºC incubator for 30 minutes then placed in a BioTek Synergy HTX. The absorbance was read at 562 nm, and the data was exported to Microsoft Excel 2016 or GraphPad Prism9 for analysis.

Based on concentrations determined through analysis, the appropriate amount of 4x laemmli sample buffer was added to each Eppendorf tube. The samples were vortexed and then boiled at 95 ºC for 10 minutes. The necessary concentration of SDS page gel was made and appropriately placed into the Western Blot container. Equal concetrations of protein were loaded for the immunoblot assay as well as the protein ladder. The gel was run for 20 minutes at 90 V or until the proteins reached the bottom of the stacking gel, then at 120 V for 100 minutes, or until the proteins reached the bottom of the gel. The gels were then transferred in 1x transfer buffer (Tris base 18.2 g, Glycine 90.0 g, and 500 mL of ultra-pure water, + 100 mL of .ethanol + 800 mL of ddH2O) with PVDF membrane at 18V for 18 hours in a 4 ºC cold room.

The PVDF membranes were then taken and blocked with 5% milk in TBST (100 mL 1x TBS + 0.025% azide + 0.05% Tween 20) at room temperature for 1 hour. After this time, the membranes were washed in TBST 3 times for 10 minutes each and the

desired antibody was placed on the membrane overnight in a 4 ºC cold room. The membranes were washed 3 times with TBST for 10 minutes each, then the mouse or rabbit secondary antibody (1:5000 in 5% milk with TBST) was placed on them for 1.5 hours at room temperature. After this time, the PVDF membrane was washed 3 times again and the ECL mixture was placed on the membrane. The ImageQuant LAS400 imager (GE Life Sciences) was used to detect the antibody signals. The antibodies used are from Cell Signaling Technology and include actin, xCT, V5, pho-H2AX, HDAC6, acetyl-tubulin, PARP cleavage, and tubulin.

1.2.5 Genome Editing Through the CRISPR/Cas9 System

CRISPR/Cas9 with a viral delivery system was used similarly to previously published techniques. Guide RNA (gRNA) was selected for HDAC6 knock-down, while PLX304 plasmid was used for xCT overexpression. The gRNA sequences were made and purchased from Genescript, while the plasmid for xCT was from DNASU. The viruses were generated with lentivirus and lipofectamine. Polybrene was added to 60 mm dishes, and the selected virus was placed in drops around the dish and then incubated overnight. The virus and polybrene was discarded on the next day, and DMEM++ medium was added to the dish and incubated for two days. This medium was replaced with DMEM + 1x antibiotics. The cells were then collected, quantified, diluted to 0.4 cells/well, and plated in 96-well plates. A gene pool was also left to grow in a 100 mm dish. After the colonies grew in the 96-well, they were collected and used for further testing. MDA231 was infected with gHDAC6, PLKO empty vector, PLX304 empty vector, and xCT-V5.

CRISPR/Cas9 was chosen over TALEN (siRNA) due to siRNA often having off-target effects.

1.2.6 Protein Immunoprecipitation (IP)

IP was completed used non-denaturing lysis buffer (20 mM Tris HCl pH 8 + 137 mM NaCL + 10% glycerol + 1% Triton X-100 + 2 mM EDTA + protease and phosphatase inhibitors). Cells were washed with ice-cold PBS in a cell culture hood, then the PBS was removed and 0.5 mL ice cold IP lysis buffer was added. The cells were scraped off the plate with a cell lifter and transferred to microcentrifuge tubes. The tubes were left on ice for 30 minutes to allow the cells to lyse and vortexed every 10 minutes. After this time, the tubes were centrifuged for 15 minutes at 14,000 g at 4 ºC. The protein concentration was determined with BCA assay, similarly to the Western Blot procedure explained previously.

Magnetic beads were washed by placing 20 µL of bead slurry in a tube on a magnetic separation rack. The buffer was carefully removed to leave the beads behind. 500 µL of ice-cold IP lysis buffer was added, and the microcentrifuge tube was vortexed and then placed back on the magnetic rack. The buffer was carefully removed from the beads. This washing process was completed twice, after which 200 µL of cell lysate was added to the beads and allowed to incubate with rotation for 1 hour in a 4 ºC cold room. The tube was placed back on the magnetic rack, and the lysate was carefully removed and placed into a clean microcentrifuge tube. The magnetic bead pellet was discarded. This was repeated until the desired amount of lysis was obtained.

On ice, 400 µL of lysate was added to a microcentrifuge tube with 3 µL of the desired antibody (primary or control). This tube was rotated overnight at 4ºC. Magnetic beads were pre-washed and the lysate + antibody mix was added to the tube with magnetic beads. The pellet and antibody was allowed to incubate with rotation for 2-4 hours in the 4ºC cold room then placed on a magnetic separation rack. The lysate was removed and placed in a new microcentrifuge tube. The magnetic beads were washed 4x with 1000 µL of 1x cell lysis buffer (no protease or phosphatase inhibitors) by gently inverting the tube 4 to 5 times. The buffer was removed between washes. The magnetic pellet was then resuspended with 50 µL 2x SDS sample buffer, vortexed, and microcentrifuged at 10,000 g for 15 seconds. The sample was then boiled at 95ºC for 10 minutes to denature the protein and separate it from the magnetic beads. After this time, the sample was briefly centrifuged at 10,000 g and placed on the magnetic separation rack. The supernatant was moved to a new tube and 20 µL was used for Western Blot.

1.2.7 RNA Extraction, Reverse Transcription, and quantitative PCR

RNA was extracted using RNeasy kit (QIAGEN). RNA lysis buffer (mixed with 2-mercaptoethanol) was added to each well of a 6-well plate. RNAse-free water was used to create a 70% ethanol mixture and placed into each well. Ethanol, lysis buffer, and cell mixture were added to a spin cartridge and centrifuged for 30 seconds at 10,000g. The supernatant was discarded, and wash buffer 1 was added to the filter cartridge as instructed in the manufacturer's manual. The tube was centrifuged, and the supernatant was discarded. This process was then repeated twice with Wash Buffer 2. RNA free

water was added to the center of the filter and allowed to sit for 1-2 minutes. The tube was then centrifuged, and the filter was discarded. The concentration of the purified RNA was determined using a NanoDrop™ 1000 (Thermo Scientific). The RNA concentration was exported into a Microsoft Excel 2016 spreadsheet, and the volumes for the master mix were calculated.

In an ice bath, the calculated amounts of master mix (RTase, Rnase inhibitor, hexamers), RNAse-free water, and sample were added to PCR tubes. The RNA was reverse-transcribed to cDNA, using a standard protocol (Thermo Fisher). Gene expression levels were determined by quantitative RT-PCR (qRT-PCR) with varying primers and SYBR Green PCR mix (Thermo Fisher). A qPCR plate was placed in an ice bath and loaded with 2.5 µL of cDNA template followed by 7.5 µL of desired master mix (5 µL 2x SYBR Green, 0.2 µL forward and reverse primer, and 2.3 µL DDW) per well. An adhesive transparent membrane was stuck to the top of the plate, which was then centrifuged for 1 minute at 1500 g. The plate was then loaded into the qPCR machine (Applied Biosystems, Thermo Fisher) and ran at the standard protocol.

1.2.8 Gene Profiling Analysis by Affymetrix Microarray

Desired cells were plated at a concentration of 0.1 million per well in a 6-well plate. The cells were allowed to grow in the incubator then treated with the desired drugs and concentrations. Once 20-30% of the cells appeared dead in a brightfield microscope, RNA lysis buffer + 2-mercaptoethanol were added to each well. RNA was extracted following the RNAeasy Kit (Qiagen) instructions and their concentrations were

determined with a Nanodrop. qRT-PCR was completed for the samples, and they were placed in labeled PCR strips and sent to Functional Genomics Core for microarray analysis. The results were analyzed to compare relative expression levels between the sensitive and resistant lines. The data were RMA normalized with Affymetrix Expression Console ver1.0. Each cell line was log2-transformed and normalized by Bayesian Factor Regresin Analysis (BFRM) [36].

1.3 Results

1.3.1 Develop and establish an *in vitro* TNBC cell model resistant to the targeted cyst(e)ine-addiction therapy

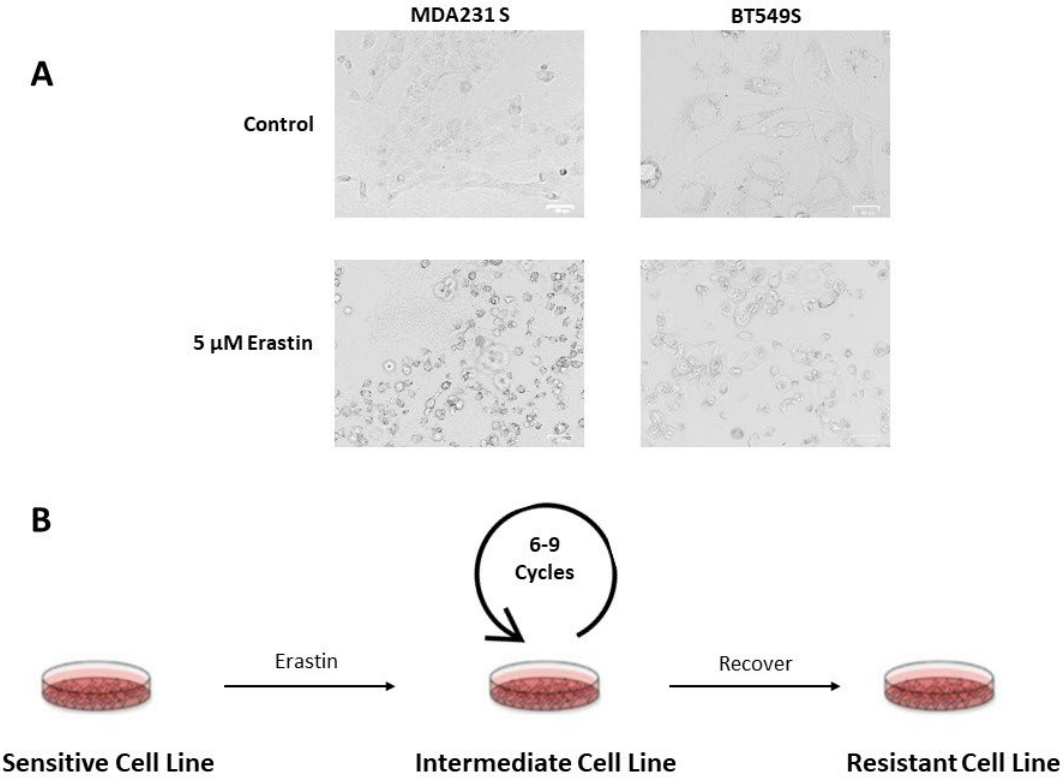

Figure 2: Scheme of establishing an *in vitro* erastin-resistant TNBC model. (A) Bright field microscopy images of original observations of MDA231 S and BT549 S in control and 5 µM Erastin treatment. (B) Scheme of developing an *in vitro* resistance model with increasing concentrations of Erastin challenges.

Our earlier report suggests that "cyst(e)ine-addiction/dependency" is a novel hallmark of a subset of triple-negative breast cancer (TNBC) [16]. Limiting cellular cyst(e)ine by targeting cystine transport or cystine deprivation induces extensive programmed necrosis in mesenchymal TNBC. The targeted cyst(e)ine-addiction could be a promising strategy to treat the cyst(e)ine-addictive cancers. Although almost all of cells were killed by the erastin treatment, a small portion of cells was repeatedly observed to

survive after a 3-day treatment of erastin (**Fig. 2A**). About 5% -10% of the cells became resistant and survived, but the rate of survival varied among different cell lines. These observations alerted us that the surviving cells might continue to proliferate and eventually outgrow the susceptible ones, so that they dominate the tumor cell population, leading to tumor relapse. This phenomenon mimics the tumor recurrences that are commonly seen in clinical settings. To that end, we plan to develop and establish an in vitro cell model resistant to the targeted cyst(e)ine-addiction therapy. Such cell model systems will be utilized to study the underlying mechanisms, which render tumor cells from cystine-addictive to cystine-independent. We developed a strategy with multiple-cycle stress (erastin) challenges to enrich the resistant cell population (**Fig. 2B**). Erastin blocks the xCT antiporter, which transports cystine into the cells, and causes programmed cell death through necrosis [16]. Sensitive TNBC cells were treated with 5 μM erastin for three days at a time. The surviving cells were collected and allowed to grow in culture. This was repeated until the majority of cells survived then the erastin concentration was increased until desired concentration. The in vitro resistant model was successfully created and both MDA231 E^R and BT549 E^R lines were able to gain resistance to 10 μM erastin after 9 cycles while HBL100 gained resistant to 5 μM after 12 cycles (**Fig. 2B**). This model was verified with Cytotoxic Fluor Assay™ and crystal violet staining (F**ig. 3A-H**). As the cells underwent necrosis at high concentrations of erastin treatment, the cell membrane burst, which caused a release of protease that could be measured. The *in vitro* erastin-resistant models MDA231 E^R and BT549 E^R weresucessfully established after 9 stress cycles. Both MDA231 E^R and BT549 E^R were able to gain resistance to 10 μM erastin, as shown by the absence of protease release (**Fig. 3A and 3C**) and normal

cell attachment on culture plates (**Fig. 3B and 3D**), while the parental lines (MDA231 S and BT549 S) quickly died at 24 hrs upon 5 µM treatment. HBL100 exhibited a weaker ability to gain erastin-resistance. After 12 stress cycles, HBL100 E^R was only able to gain resistant to 5 µM, but not 10 µM (**Fig. 3E and 3F**). This might be caused by the extreme erastin-sensitivity of the parental HBL100 cells. Nevertheless, all three in vitro cell

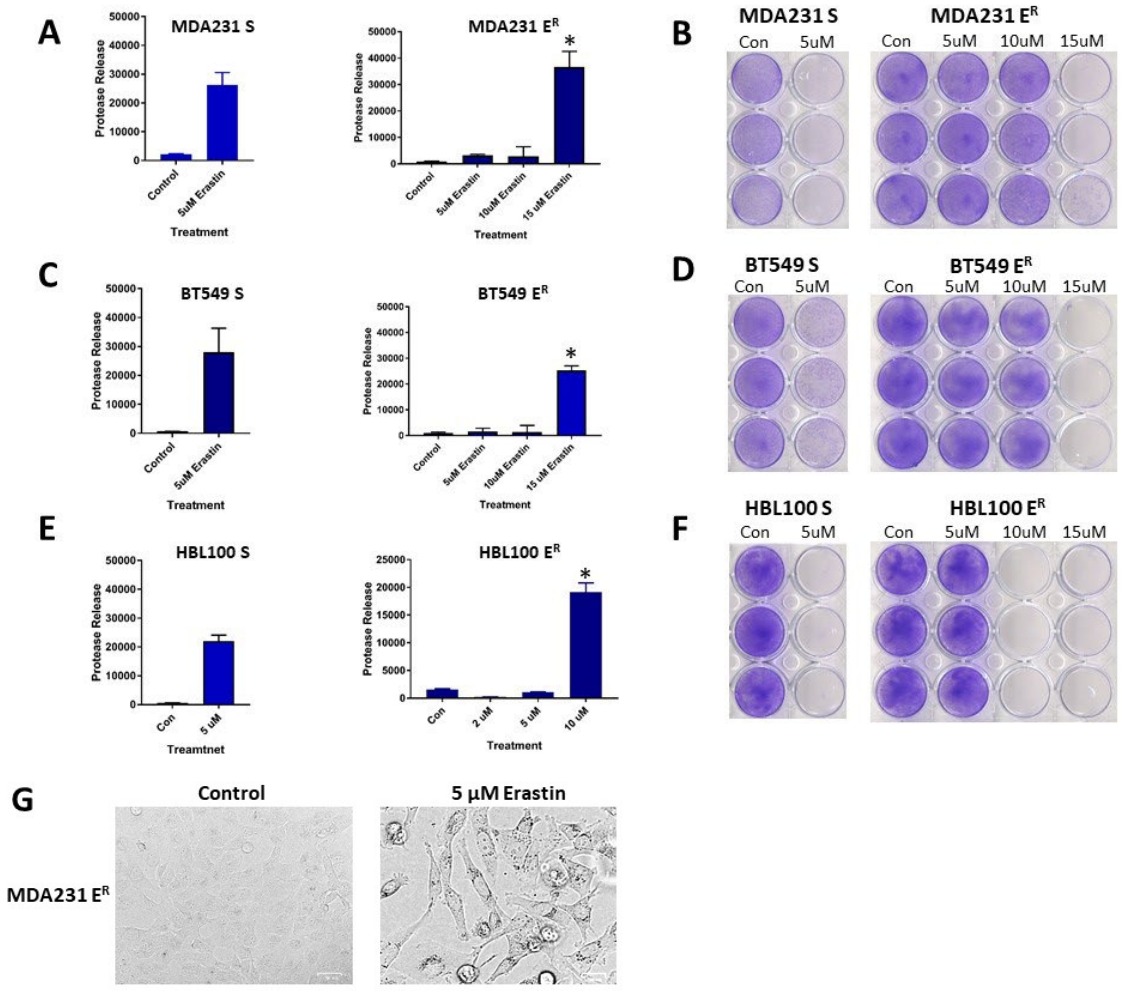

Figure 3: Cell survival of resistant cells versus their parental sensitive cells in response to erastin treatments. The rate of cell death measured by the Cytotox Fluor assay in three resistant cells versus their parental cells under different doses of erastin treatments (p=<0.0001) (A, C, E). Crystal violet staining of all three resistant models versus their parental cells under stress (B, D, F). Cell morphology of MDA231 E^R cells under control or erastin treatment (G).

systems have been successfully established to gain a certain degree of erastin-resistance in comparison to their parental cysteine-addictive counterparts.

Alternatively, an *in vitro* resistance model, in which cells gain direct resistance to cysteine deprivation in the medium instead of blockage of cystine transport was also developed. Normal cell culture medium contains 200 μM cystine. Originally the MDA-MB-231 S cells could not survive in media with only 2 μM cystine. In order to generate cystine-independent cells, we stressed the cells with 12 cycles of sequential treatments from 2 μM cystine to 0.2 μM cystine containing culture medium. The cells were not able to survive in medium that lacked cysteine completely. This line, termed MDA-MB-231 C^R, was able to survive upon 2 μM erastin treatment, but not higher doses of erastin (**Fig. 4A, right panel**), while the parental MDA-MB-231 S cells showed high sensitivity of erastin and did not survive from any doses of erastin treatment (**Fig. 4A, left panel**). On the contrary, MDA-MB-231 E^R cells were resistant to all tested doses of the erastin (**Fig. 4A, middle panel**). Reciprocally, the MDA-MB-231 E^R cells were able to survive in 1 μM cysteine medium as the C^R cells while parental MDA-MB-231 underwent necrosis at the same concentration (**Fig. 4B**). However, both derived cell line resistant lines, MDA231 E^R and MDA231 C^R, underwent cell death in medium completely deprived of cysteine as the parental MDA231 S (**Fig. 4C**). Thus, the the MDA-MB-231 C^R cell model shows a weaker erastin-resistance, suggesting different therapeutic interventions might promote various resistance mechanisms.

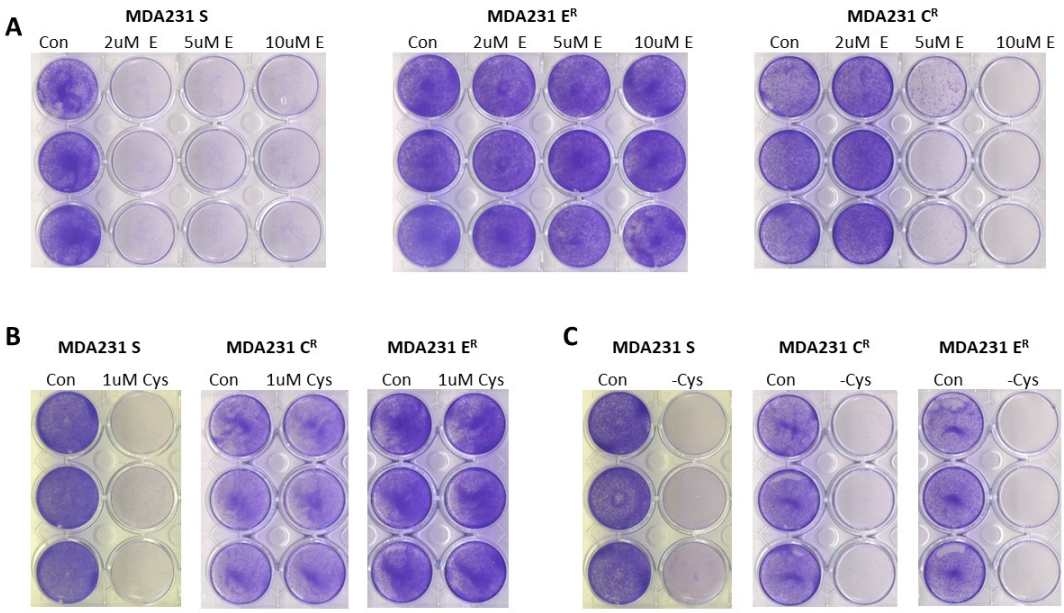

Figure 4: Differential responses of MDA231 S, MDA231 E^R, and MDA231 C^R to erastin and direct cystine deprivation. Survival of indicated cells upon different doses of erastin (**A**), 1 μM cysteine (**B**) or complete cysteine deprivation treatments (**C**).

1.3.2 Increased expression of cystine antiporter does not contribute to the erastin-resistance

Using the *in vitro* resistance model, the mechanism of resistance was thought to involve the cysteine metabolism pathway. Dysregulation of key components of this pathway, including GCLC, GCLM, and xCT, could cause potential causes resistance to erastin. Previous studies had suggested that erastin is a direct inhibitor of the xCT antiporter to limit the intake of cystine [37], therefore, an increase of xCT expression could potentially cause cells resistant to the erastin treatment. The RNA and protein level of the xCT antiporter in both the resistant and sensitive cells was examined. The RNA expression of xCT was found increased in the MDA231 E^R line, but not in the other resistant lines, when compared to their erastin-sensitive counterparts (**Fig. 5A**). Further, Western blot analysis confirmed that the xCT protein was increased in MDA-MB-231 E^R

cells, but not in parental MDA-MB-231 S cells (**Fig. 5B**). Interestingly, we found that two bands were detected at sizes about 300 kD and 27 kD when using the anti-xCT antibody in the immunoblotting analysis. According to the amino acid sequence of the xCT gene, the molecular weight of xCT protein should be about 27 kD. To validate that both these bands are xCT protein, the C-terminal V5-tagged xCT expression construct was used to overexpress the xCT protein in MDA231 S cells by viral infection. Using the anti-V5 antibody, we found that both the 300 kD and 27 kD bands were seen in the V5-xCT-infected cells but not in the empty-vector-infected cells, suggesting that both bands represent xCT protein (**Fig. 5C**). Since xCT is a plasma membrane protein, we hypothesize that the high molecular weight of xCT protein is due to more advanced post-translational modifications and that it was not denatured by the protein lumini buffer. Next, we examined whether upregulation of the xCT protein contributes the erastin-resistance in MDA-MB-231 E^R cells. The empty vector and V5-xCT overexpressed MDA-MB-231cells were tested for the response to cystine depletion by erastin. Both lines were subjected to 5 μM erastin treatment for 24 hours then tested by the CytoTox Fluor™ Assay. We observed that the V5-xCT expressed cells died faster than the vector-only, which was indicated by a higher level of protease released in V5-xCT cells (**Fig. 5D**). Our data suggests that the xCT protein undergoes post-translational modifications, but that its increase does not contribute to the erastin-resistance.

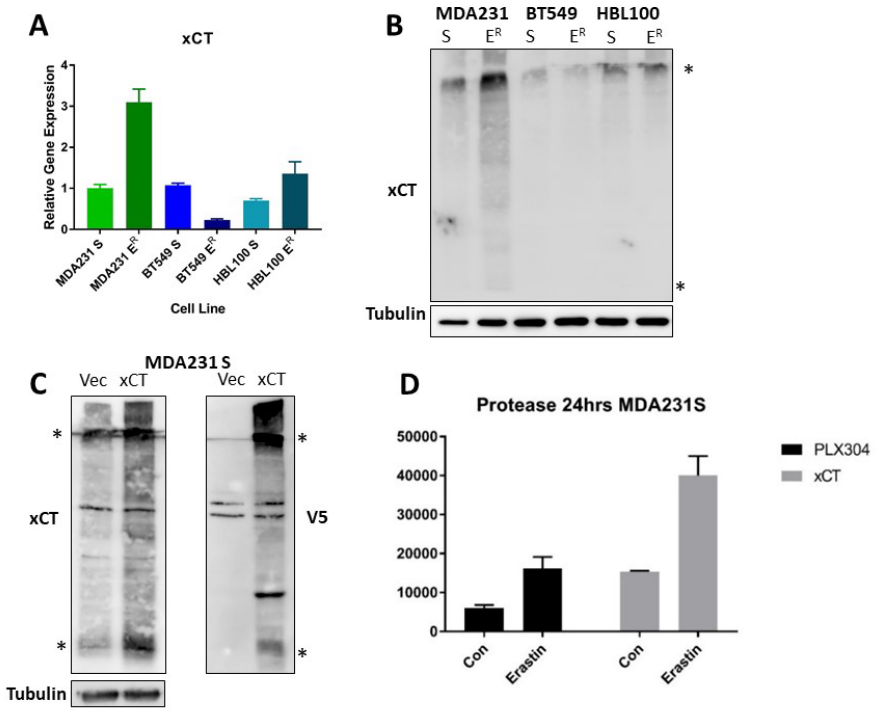

Figure 5: Increased xCT does not contribute to the erastin resistance. xCT expression levels from qPCR (A) and Western Blot (B) of three parental lines and three *in vitro* resistance models. The astericks show the two xCT bands that were found. Western blot validation of xCT-V5 tagged over-expression via infection (C). Protease release measurement using CytoTox Fluor™ Assay at 24 hours of 5 µM Erastin treatment in the vector and xCT over-expressed lines (D).

1.3.3 Identify epigenetic sensitizers with an epigenetics compound library screening to overcome erastin resistance

TNBC is found to commonly recur after chemotherapy treatment [4, 5]. These recurrent tumors have gained resistance to the previous treatment used and require a new therapy. Clinically, recurrent TNBC tumors are treated with combinations of known drugs to attempt to overcome their resistance to the first treatment [4-6]. One kind of combination therapy is to use a sensitizer that causes the recurrent tumor to undergo cell death from the previously used drug. In recent studies, epigenetic alterations have been suggested as mechanisms of tumor drug resistance [38, 39]. Small, reversible chemical modifications to DNA or histones, such as methylation or acetylation, allow cancer cells

to regulate their genes expression to evolve and gain adaptations to stresses. By targeting these epigenetic mechanisms, recurrent cancers have been found to become sensitized to certain therapies and treatments [38, 40].

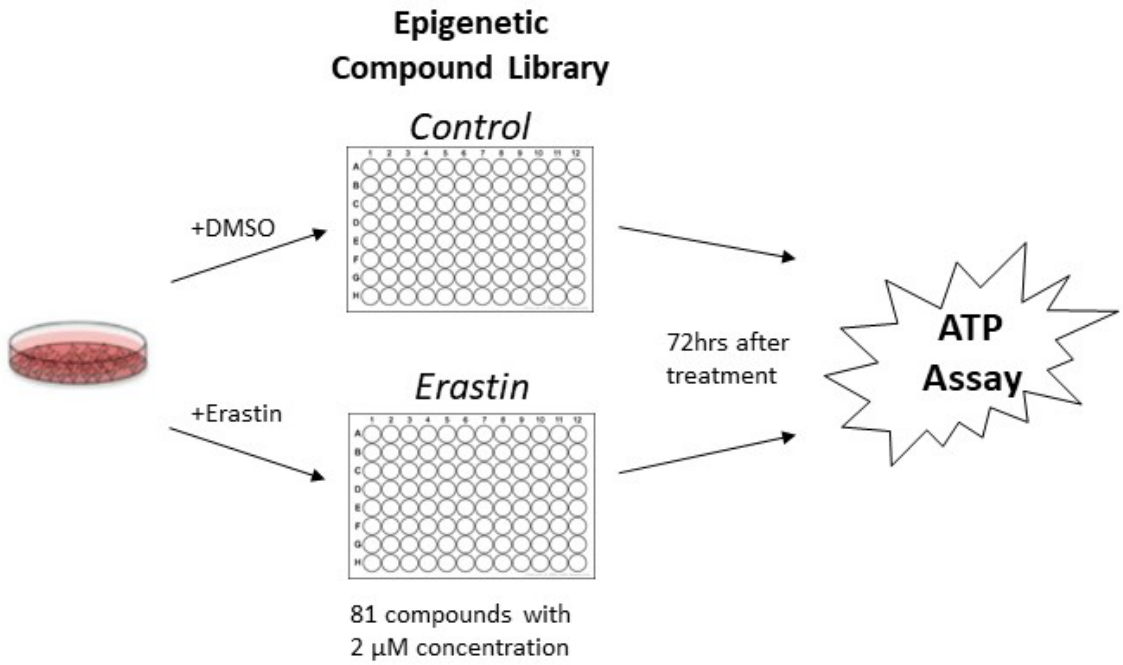

Figure 6: Methodology for epigenetic drug screening assay using *in vitro* resistance model. The epigenetic drugs from Cayman Chemical were prepared at a 2 µM final concentration in the control and erastin plates. MDA-MB-231 cells in a desired cell number were plated in the erastin plate with 5 µM erastin, while cells with DMSO were added to the control plate. Cells were monitored daily with microscopy and then subjected to ATP assay after 72 hours.

To identify potential epigenetic sensitizers to overcome the drug resistance of our developed *in vitro* erastin resistance models, we designed a strategy of an epigenetic compound library screen, as depicted in **Fig. 6**. This screening epigenetic compound library was purchased from Cayman Chemical. MDA-MB-231 E^R cells were plated in a control plate that contained the selected compounds plus DMSO, and in the erastin plate that contained 5 μM erastin instead of DMSO. After 72 hours, cell survival was measured by the ATP level using the CellTiter Glo assay (**Fig. 7A**). The compounds with strong synergetic death effects on cells with erastin but no obvious effects in the control condition were considered to be potent sensitizers and selected for further validation.

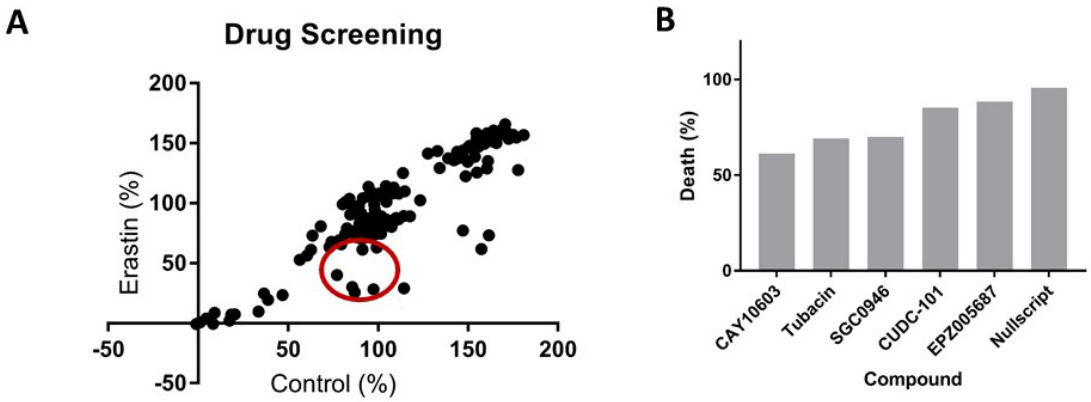

C

Drug	Usage	Difference (%)
CAY10603	Histone Deacetylate (HDAC6) Inhibitor	61.21543349
Tubacin	HDAC6 Inhibitor	69.11042521
SGC0946	Protein methyltransferase (PMT) inhibitor	69.91332658
CUDC-101	HDAC and EGRF (HER2) Inhibitor	85.22235291
EPZ005687	Histone Methyltransferase (HMT) Inhibitor	88.45308166
Nullscript	HDAC Inhibtor inactive analog	95.74542703

Figure 7: Epigenetic compound library screen in MDA-MB-231 E^R cells. Results from epigenetic drug screening comparing the percentage of living cells in control plate and erastin combination plate through the ATP assay (A). Six treatments that caused the highest amounts of cell death were selected and their targets were determined (B and C).

Compounds with high toxicity to cells in either the control or erastin condition were ruled out.

After data analysis, six potent epigenetic sensitizers were identified to induce extensive cells death (~ 70% - 95%) in MDA-MB-231 E^R cells when co-treated with erastin, but not treated by themselves (**Fig. 7B and 7C**). Four of the six compounds are histone deacetylate (HDAC) inhibitors while the other two are inhibitors of histone methyltranferases. To validate our screen results, two identified methyltransferase inhibitors (EPZ005687 and SGC0946) were tested on the erastin-resistant TNBC models. EPZ005687 inhibits the enhancer of *zeste homolog 2 (EZH2*) while *SGC0946* inhibits *disrupter of telomeric silencing-like 1 (DOT1L*) [41]. The CellTiter Glo assay was used to measure cell survival similarly to the epigenetic library screening. Both compounds at 4 μM in combination with 5 μM erastin were able to overcome resistance in MDA232 E^R (**Fig. 8A and 8B**), while either drug by themselves were not able to cause cell death at the given concentration. The results show significant death ($p=<0.0001$) for the combined treatments. We further tested the effects of these two sensitizers in two other erastin-resistant TNBC BT549 E^R and HBL100 E^R models. Similar synergetic death effects by identified sensitizers were observed in different erastin-resistant cells (**Fig. 8C-8F**).

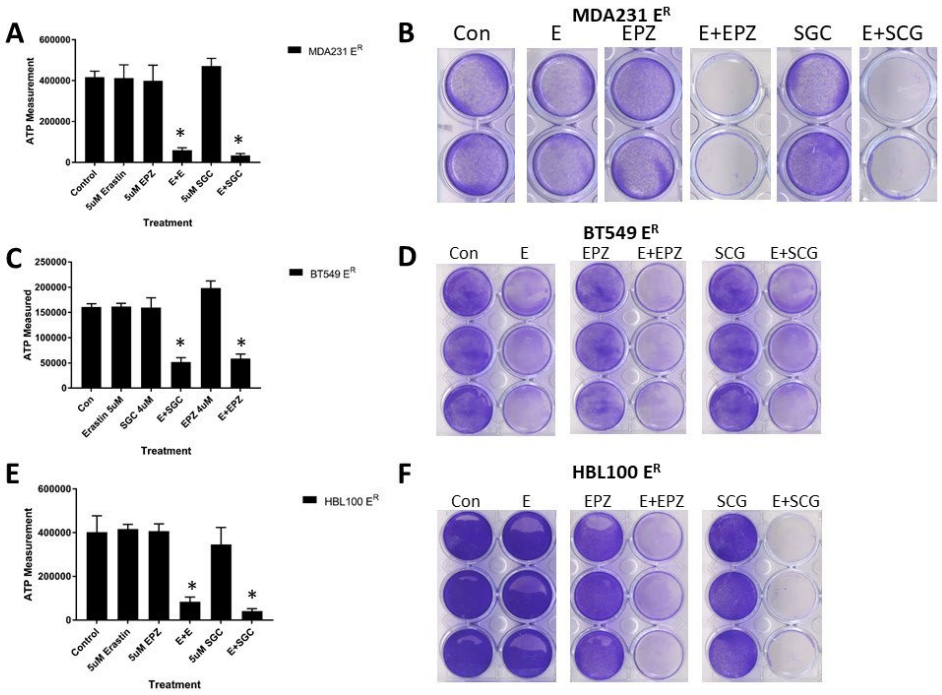

Figure 8: Validation of epigenetic drug screening on all six lines using two of the treatments that caused the highest amount of cell death in combination with erastin. The ATP assay at 24hrs was used to measure the living cells. MDA231 E^R and BT549 E^R didn't survive in 5 µM Erastin plus 4 µM EPZ005687 (p=<0.0001) or in 5 µM erastin plus 4 µM SGC0946 (p=<0.0001) (A and C). HBL100 E^R also didn't survive 5 µM erastin plus 4 µM EPZ005687 (p=0.0052) or in 5 µM erastin plus 4 µM SGC0946 (p=<0.0001) (E). Crystal violet staining at 48 hrs was used to validate the assay (B, D, F).

1.3.4 HDAC6 is not the direct molecular target of tubacin in tubacin-mediated synthetic lethality of cysteine addiction

Inhibition of general HDAC activity have been found to increase the acetylation of histones, cause cancer cell cycle arrest, reduce angiogenesis, and modulate the immune response when used as a cancer treatment [42]. Three of the top hits from the epigenetic library screening were HDAC6 inhibitors (**Fig. 7B and 7C**). Surprisingly, Nullscript, an inactive HDAC inhibitor analog, had the highest synthetic-lethal effects with erastin on the resistant tumor cells. Nevertheless, we focused the HDAC6 and chose a potent inhibitor of HDAC6, tubacin, and determine the role of HDAC6 in the erastin resistance in our *in vitro* erastin resistant TNBC models. The combination treatment of tubacin and

erastin was tested at 5 µM concentrations on the MDA231 E^R line, compared to each drug alone. The combination treatment induced extensive cell death in MDA231 E^R cells, but each drug alone did not (**Fig. 9A and 9B**). Furthermore, we found that the combined erastin and tubacin induced similar cell death in two other erastin-resistant models, BT549 E^R (**Fig. 9C and 9D**) and HBL100 E^R (**Fig. 9E and 9F**). These results suggest that the HDAC6 inhibitor tubacin is able to overcome the erastin resistance and that the HDAC6-mediated epigenetic regulation might be the underlying mechanism of erastin resistance.

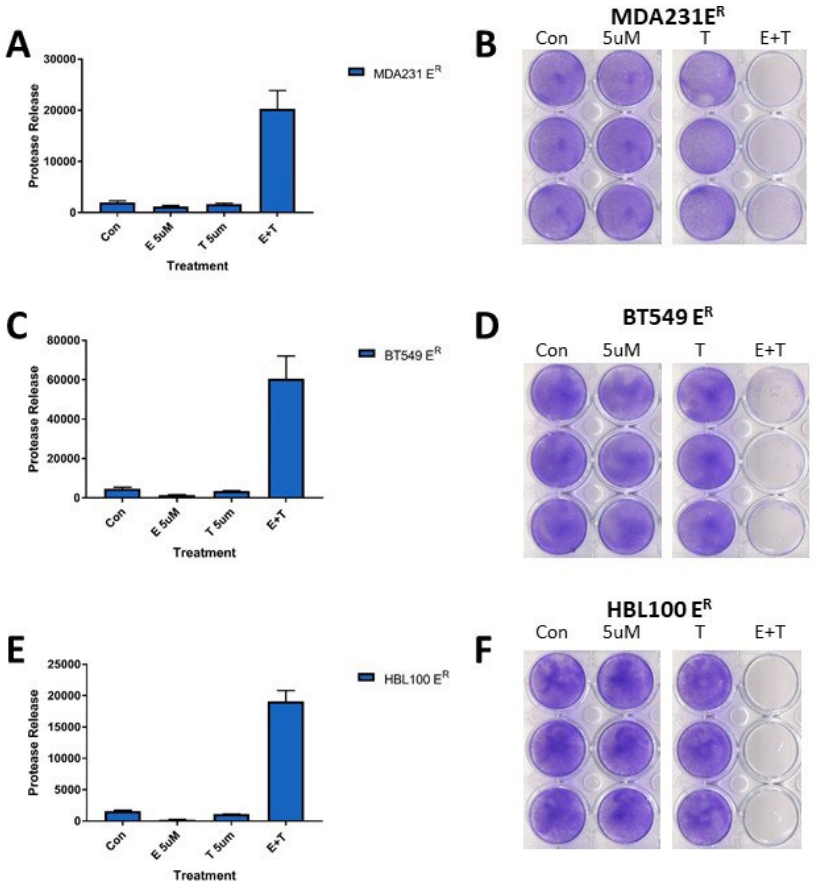

Figure 9: Tubacin induced synthetic lethality in erastin-resistant TNBC models. Protease release was measured by CytoTox Fluor™ Assay at 24 hours in MDA231 E^R (**A**), BT549 E^R (**C**), and HBL100 E^R (**E**) resistant models treated with DMSO, 5 µM Erastin, 5 µM Tubacin, and combination treatments (p=0.0061, p=0.0011, and p=0.0007, respectively). Crystal violet staining at 48 hrs was used to validate the assay (**B, D, and F**).

Tubacin has been shown to target HDAC6 specifically, which is a member of the HDAC class 2 and regulates transcription [42]. With this in mind, we furthered our study by determining the expression levels of HDAC6 in each cell line and resistance model by Western blot analysis. There was an increased expression of HDAC6 in MDA231 E^R, when compared to parental MDA231 S cells, but not increased in the other two erastin-resistant models (**Fig. 10A**). Since HDAC6 was highly expressed in the MDA231 E^R line, we hypothesized that up-regulation of HDAC6 might lead to an increase of erastin resistance and that knockdown of HDAC6 expression would overcome the resistance. We tested to knockdown HDAC6 expression in MDA231 E^R cells with the CRISPR/Cas9 approach. The resulting gHDAC6 cells and the control vector cells were tested for the sensitivity of erastin, as well as the combination treatment with tubacin. The protein levels of HDAC6 in the vector and gHDAC6 cells under 5 μM erastin, 5 μM tubacin, and erastin plus tubacin combination treatment were determined by Western blotting (**Fig. 10B**). Small guide RNA of HDAC6 mediated a lower HDAC6 expression but did not fully knock out the expression of HDAC6 in the gHDAC6 cells, in comparison to the vector cells. However, we observed that the acetylation of tubulin, the substrate of HDAC6, was significantly increased in gHDAC6 cells, and that the level of acetylated tubacin was similar to that in tubacin-treated vector cells (Fig 10B). We examined and compared the sensitivity of the vector and gHDAC6 cells to cellular cysteine depletion by erastin. Unexpectedly, we observed that the gHDAC6 cells did not acquire more

sensitivity to erastin when compared to the vector cells indicated by no significant protease releasing (**Fig. 10C and 10D**). On the contrary, the gHDAC6 were also resistant to the erastin plus tubacin treatment in comparison with the vector cells (**Fig. 10C and 10D**). These data indicated that the silencing of HDAC6 expression did not mimic the inhibitory role of tubacin. Thus a new an unknown target inhibited by tubacin may be present in cells to mediate synthetic-lethal effects with erastin.

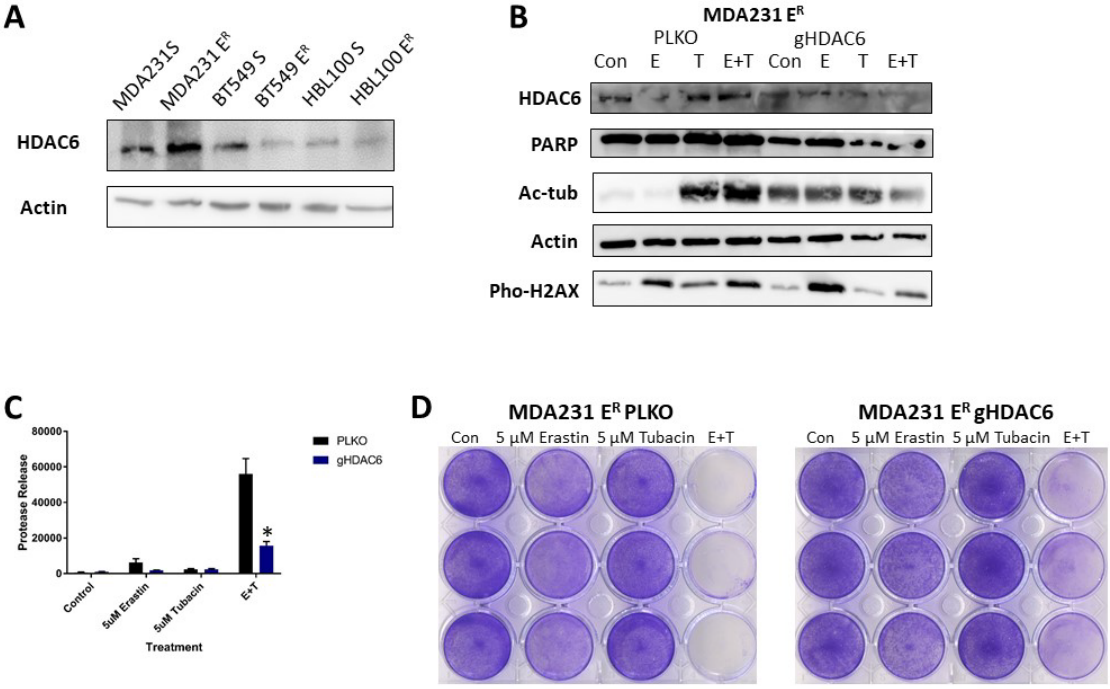

Figure 10: (**A**) **The protein expression of HDAC6 in three pairs of sensitive and erastin-resistant cells**. (**B**) Western blot analysis of indicated protein in MDA231 E^R vector and gHDAC6 cells under the control, 5 µM erastin, 5 µM tubacin, and the combination (E+T) treatments at 24 hrs. (**C**) Relative protease release (p=0.0089) was measured by the CytoTox Fluor™ Assay at 24 hrs in the vector and gHDAC6 cells under the same treatment. (**D**) Cell survival was examined by crystal violet staining.

1.3.5 Understanding the molecular mechanisms of the drug resistance by gene expression profiling analysis

The differences in gene expression levels between sensitive and resistant models could lead to the discovery of potential therapeutic targets. Total RNA samples in

triplicates were prepared with an RNA extraction kit (Qiagen) from three pairs of sensitive and erastin-resistant cells. The RNA concentrations were determined by Nanadrop™ and sent to Functional Genomics Core for processing. The expression data were normalized by RMAexpress software and log2 transformed. Level of gene expression in the erastin-resistant cells were zero-transformed to those of parental erastin-sensitive cells. The data was further clustered by Cluster 3.0, and the heatmap of the gene expression among different cells was viewed by Java TreeView (**Fig 11A**). The heatmap of gene expression profile showed hundreds of genes in MDA-MB-231 E^R and BT549 E^R cells that differed by two-fold or more from their parental erastin-sensitive cells (**Fig. 11A**). HBL100 E^R cells had much fewer gene expression differences from HBL100 S cells. This might be because HBL100 E^R cells were only able to gain resistance to the 5μM treatment.

To that end, the gene expression profiles from only MDA231 and BT549 cell models were used for further analysis (**Fig. 11B**). Besides the hundreds of genes that were either upregulated or downregulated in individual erastin-resistant cells, 156 genes were up-regulated and 334 genes were down-regulated in both erastin-resistant models by over two-fold (**Fig. 11C**). Of the up-regulated group, six genes were selected to validate the microarray data by RT-qPCR. Five genes of these genes, except DNMT3A, were dramatically elevated in MDA-MB-231 E^R and BT549 E^R cells when compared to those parental cells (**Fig. 12A-12E**). The expression of these genes was less changed in HBL100 E^R cells. CBS has a 40-fold increase in MDA231 E^R and 500-fold increase in BT549 E^R **(Fig. 12 A)**. The CBS gene codes cystathionine beta synthase that generates

cystathionine from homocysteine and serine via the transsulfuration pathway. Cystathionine is further cleaved into cysteine. CBS plays a pivotal role in the decision of converting methionine to cysteine. Upregulation of CBS gene the erastin-resistant cells may rewire the source of cellular cysteine from the methionine transsulfuration pathway (**Fig. 1**). In that case, the erastin-resistant cells had sufficient cysteine to counteract the blockage of cystine transport by erastin and exhibited the resistance of erastin.

Two genes, p14 and p16, are both encoded in the same gene locus CDKN2A, which interact two important tumor suppressors, p53 and Rb, regulate cell cycle, survival, and differentiation. The CDKN2A gene locus is commonly found to be deleted, mutated, or methylated in cancer [44, 45]. A recent study has found epigenetic changes in the CDKN2A locus that were associated with a difference in gene expression of encoded proteins [43]. The hypermethylation of this locus could lead to alternative reading frames (ARF) and silent p14 and p16 expressions. We found that both MDA-MB-231 S and BT549 S had extremely low levels of p14 and p16 expression. However, p14 was increased 150-fold in MDA231 E^R cells and 2000-fold in BT549 E^R cells. Similarly, p16 was upregulated to 40-fold and 5000-fold in MDA231 E^R and BT549 E^R cells, respectively (**Fig. 12 B and C)**. HBL100 S cells had high basal level of p14 and p16 expression with a minimal increase in HBL100 E^R cells. Ink4a/p16 is a tumor suppressor that arrests the cell cycle at G1 in normal cells by inhibiting the phosphorylation of Rb by CDK2 and CDK4 [44, 45]. Arf/p14 is a smaller protein from an alternative reading frame of CDKN2A that sequesters MDM2, the ubiquitin E3 ligase of p53, to prevent p53 from being broken down and activating the p53 pathway [44]. Therefore, a high level of p14

will accumulate wild type p53 in cells and induce cell growth arrest or apoptosis. Both MDA-MB-231 and BT549 cells have mutant p53, so these cells are tolerant to high p14 expression. However, HBL100 cells contain a wild type p53. We found HBL100 hardly achieved resistance to high dose of erastin. These observations suggest that reactivation of CDK2A gene locus is likely a common mechanism to gain the erastin resistance.

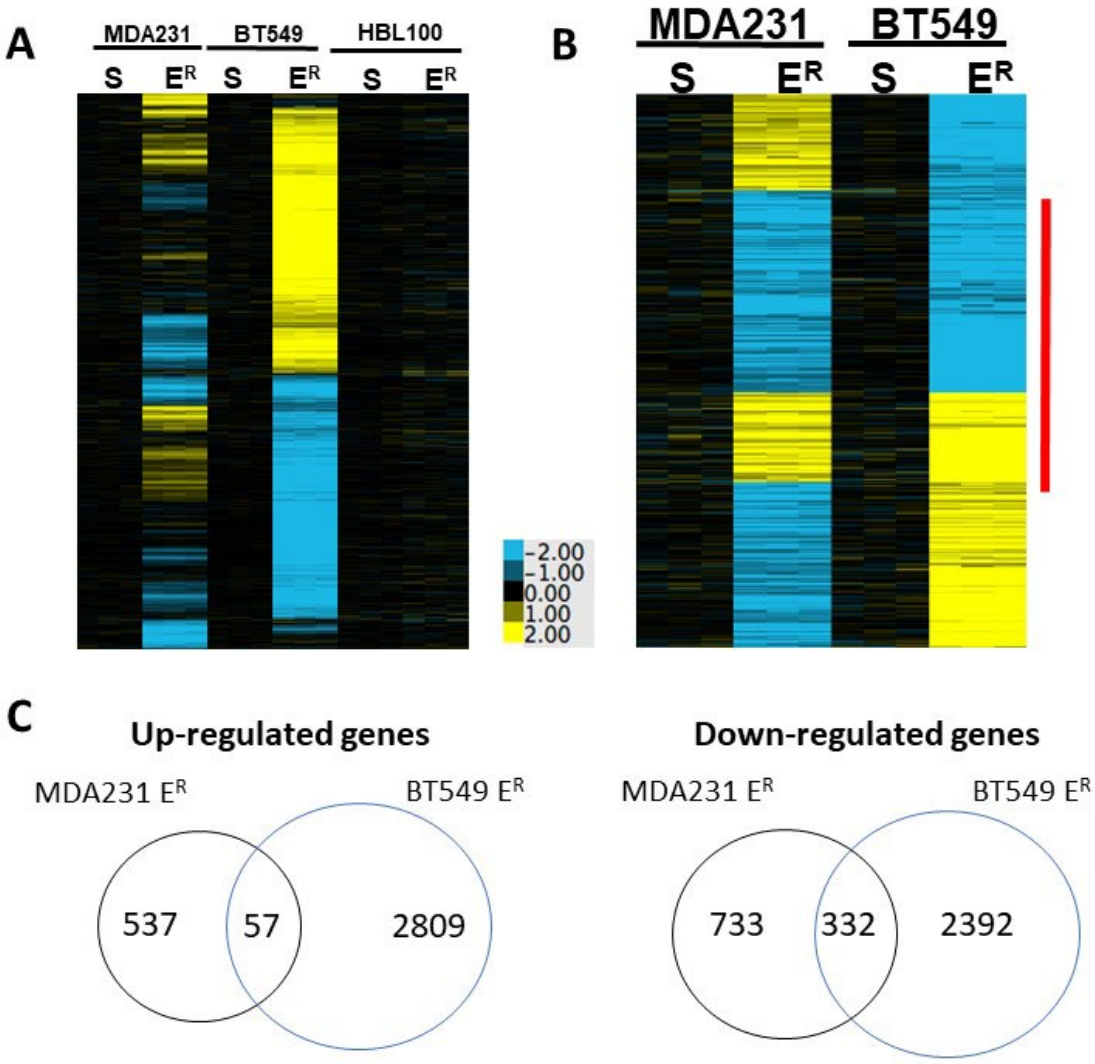

Figure 11: Gene expression profiling by microarray analysis. Heatmap viewing of gene expression changes in three erastin resistance TNBC models that have a two-fold or more difference from their parental cells (**A**). Comparison of genes that are up-regulated or down-regulated in both MDA231 and BT549 E^R lines versus their parental lines (**B and C**).

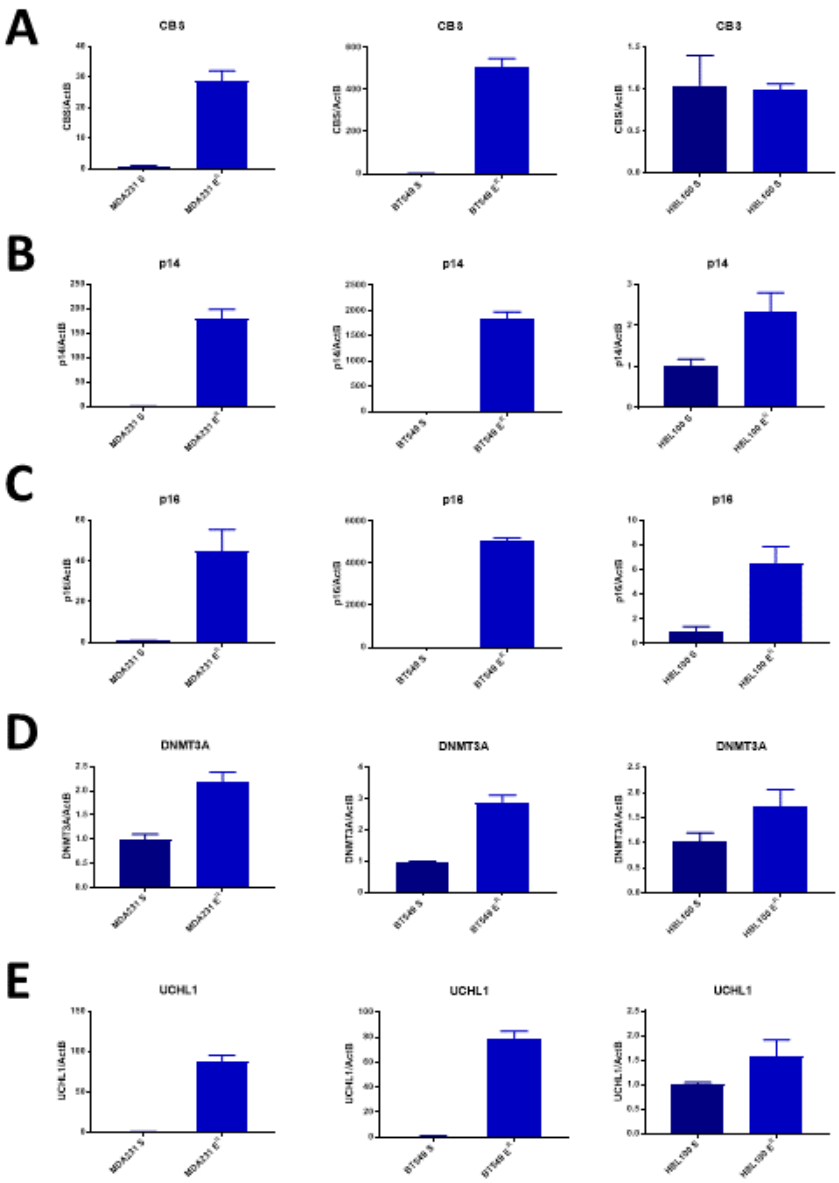

Figure 12: qPCR validation of five genes that were up-regulated in both MDA231 E^R, BT549 E^R, and HBL100 E^R (A-E).

DNMT3A, is responsible for DNA methylation and therefore gene expression. It has recently been associated with tumorigenesis and is commonly found to be mutated in cancers [46]. An increase of DNMT3A expression in our resistant model would suggest that DNA methylation is involved in drug resistance adaptation. The ubiquitin carboxyl-

terminal hydrolase 1 (UCHL1) has an 80-fold increase in both erastin-resistant models (**Fig. 12 E).** UCHL1 is thought to break down unneeded proteins, but the exact function is still being determined [47]. In cancer, an overexpression of this gene has been linked to invasive abilities [47].

Taken together, our microarray analysis indicated that cells undergoing the erastin resistance are undergoing large gene expression changes. Further analysis may discover the underlying mechanism of the erastin resistance and identify potential targets to eliminate the drug resistance.

1.4 Conclusion

Multiple in vitro resistance models were successfully created and tested with erastin treatments. The cell lines resistant to erastin were compared to a cysteine deprivation model to ensure the drug was binding to the xCT antiporter and hindering the cysteine metabolism pathway. This comparison was successful as the erastin resistant model behaved similarly to the cysteine deprivation model in low or absent cysteine concentrations. Since erastin targets the xCT antiporter, gene and protein expression level were tested and found to be higher in the MDA231 E^R line, but not in the other resistant models. Up-regulation of this gene in MDA231S was successful, but it didn't cause resistance. It can be concluded that xCT up-regulation is not the mechanism of resistance for this model.

Epigenetic drug screening results led to the potential of HDAC6 as a target for overcoming resistance. Tubacin was used as an HDAC6 inhibitor in combination with erastin to successfully overcome resistance in all three resistance lines, but overexpression of this gene was only seen in MDA231 E^R. Additionally, knock-down of HDAC6 didn't lead to a loss of resistance in the MDA231 E^R line, suggesting that this epigenetic target would not lead to an effective in vivo treatment.

Microarray results lead to five new genes that could potentially be targeted to overcome resistance. These genes were successfully validated with qPCR to ensure they were up-regulated in the BT549 E^R and MDA231 E^R lines. Future studies are needed to assess whether manipulation of these genes would lead to a loss of resistance. If successful, in vivo studies with claudin-low TNBC tumors can be applied.

A Supplemental Data

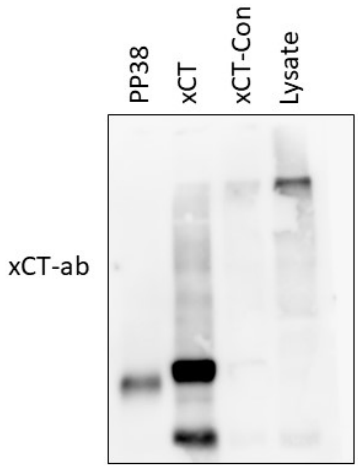

Supplemental 1: Protein immunoprecipitation results using xCT and PP38 antibody overnight with magnetic beads. The resulting proteins were subjected to BCA for concentration determination and used for Western Blot. The first lane is the protein that was incubated with PP38. The second lane is the protein incubated with xCT antibody while the third lane is the lysate collected after incubation and the fourth lane was the lysate collected before xCT incubation.

Immunoprecipitation assay was completed to attempt to isolate the xCT protein from an MDA231 E^R sample (**fig. 12**). PP38 antibody was used as a comparison. After the sample was incubated overnight with xCT antibody, the lysate was collected and used as a comparison in the western blot (lane 4). Once the beads were separated from the protein, the remaining lysate after washing was collected to ensure the xCT protein was collected (lane 3). The bands of the isolated xCT protein appear at 55kD and 27KD which would correspond to the heavy and light chains; however, previous studies, and the lower band of our work, have found xCT around 27kD which made it difficult to conclude that the lower band was the correct xCT band.

Primer	DNA Sequence
Actin-For	CACTCTTCCAGCCTTCCTTC
Actin-Rev	GGATGTCCACGTCACACTTC
xCT-For	GGACAAGAAACCCAGGTGGT
xCT-Rev	CTTCTTCTGGTACAACTTCCAGT
DOT1L-For	GCCCAAGAAGAACCAAACTGC
DOT1L-Rev	GTGAGGGGATCTGTAGGCAT
CBS-For	CGACTCAGTGCGGAACTACA
CBS-Rev	GGCTTCTTCTCCGTGAGGTC
UCHL1-For	ACGAATGCCTTTTCCGGTGA
UCHL1-Rev	GACTTCTCCTTGCTCACGCT
p14-For	GGGTTTTCGTGGTTCACATC
p14-Rev	GGCGCTGCCCATCATCAT
p16-For	GCCCAACGCACCGAATAGTT
p16-Rev	CACGGGTCGGGTGAGAGT
DNMT3A-For	CCCGCTACTTCTGGGGTAAC
DNMT3A-Rev	CTTGGCTATCCTGCCATGCT

Supplemental 2: List of primers used in qPCR and their respective sequences

B References

1. Bray, F., et al., *Global cancer statistics 2018: GLOBOCAN estimates of incidence and mortality worldwide for 36 cancers in 185 countries.* CA: A Cancer Journal for Clinicians, 2018. **68**(6): p. 394-424.
2. Ogrodzinski, M.B., Jamie; Lunt, Sophia;, *Deciphering metabolic rewiring in breast cancer subtypes.* Translational Research, 2017. **189**: p. 105-122.
3. Kang, S.P., M. Martel, and L.N. Harris, *Triple negative breast cancer: current understanding of biology and treatment options.* Current Opinion in Obstetrics & Gynecology, 2008. **20**(1): p. 40-46.
4. Foulkes, W.D.S., Ian E.; Reis-Filho, Jorge S.;, *Current Concepts Triple-Negative Breast Cancer.* The New England Journal of Medicine, 2010. **363**: p. 1938-48.
5. Dias, K.D.-G., Anna; Hallett, Robin; Wu, Ying; Hassell, John; et. al., *Claudin-Low Breast Cancer; Clinical and Pathological Charateristics.* PLOS One, 2017. **12**(1).
6. Long, J.-P., X.-N. Li, and F. Zhang, *Targeting metabolism in breast cancer: How far we can go?* World journal of clinical oncology, 2016. **7**(1): p. 122-130.
7. Perou, C.M., *Molecular Stratification of Triple-Negative Breast Cancers.* Oncologist, 2010. **15**: p. 39-48.
8. Desantis, C.E., et al., *Breast cancer statistics, 2017, racial disparity in mortality by state.* CA: A Cancer Journal for Clinicians, 2017. **67**(6): p. 439-448.
9. Foulkes, W.D.S., I. M.; Chappuis, P.O.; et. al., *Germline BRCA mutations and a basal epithelial phenotype in breast cancer.* Journal of the National Cancer Institute, 2003. **95**: p. 1482-5.
10. Weigelt, B.B., F.L.; Reis-Filho, J.S.;, *The contribution of gene expression profiling to breast cancer classification, prognostication and prediction: a retrospective of the last decade.* Journal of Pathology, 2010. **220**: p. 263-80.
11. Hanahan, D. and R.A. Weinberg, *The Hallmarks of Cancer.* Cell, 2000. **100**(1): p. 57-70.
12. Hanahan, D. and Robert a. Weinberg, *Hallmarks of Cancer: The Next Generation.* Cell, 2011. **144**(5): p. 646-674.
13. Warburg, O., *On the Origin of Cancer Cells.* Science, 1956. **123**(3191): p. 309-314.
14. Ward, P.T., Craig, *Metabolic Reprogramming: A Cancer Hallmark Even Warburg Did Not Anticipate.* Cancer Cell, 2012. **21**(3): p. 297-308.
15. Bensaad, K.T., Atsushi; Selak, Mary; et al, *TIGAR, a p53-Inducible Regulator of Glycolysis and Apoptosis.* 2006. **126**(1): p. 107-120.
16. Tang, X., et al., *Cystine addiction of triple-negative breast cancer associated with EMT augmented death signaling.* Oncogene, 2016. **36**(30): p. 4235–4242.
17. Le, A.L., Andrew; Hemaker, Max; Sminu, Bose; et al, *Glucose-Independent Glutamine Metabolism via TCA Cycling for Proliferation and Survival in B Cells.* Cell 2012. **15**(1): p. 110-121.
18. Lukey, M.K., William; Cerione, Richard;, *Targeting amino acid metabolism for cancer therapy.* Drug Discovery Today, 2017. **22**(5).

19. Olivares, O.D., J. Henry M.; King, Ayla; Gottlieb, Eyal; Halsey, Christina;, *Research into cancer metabolomics: Towards a clinical metamorphosis.* Seminars in Cell and Developmental Biology, 2015. **43**: p. 52-64.
20. Altman, B.J., Z.E. Stine, and C.V. Dang, *From Krebs to clinic: glutamine metabolism to cancer therapy.* Nature Reviews Cancer, 2016. **16**: p. 619.
21. Stipanuk, M.H., et al., *Mammalian Cysteine Metabolism: New Insights into Regulation of Cysteine Metabolism.* The Journal of Nutrition, 2006. **136**(6): p. 1652S-1659S.
22. Habib, E.L.-M., Katja; Lin, Han-Xin; Singh, Gurmit;, *Expression of xCT and activity of system xc− are regulated by NRF2 in human breast cancer cells in response to oxidative stress.* Redox Biology, 2015. **5**: p. 33-42.
23. Lanzardo, S., et al., *Immunotargeting of Antigen xCT Attenuates Stem-like Cell Behavior and Metastatic Progression in Breast Cancer.* Cancer Research, 2016. **76**(1): p. 62-72.
24. Nelson, D.C., Michael;, *Lehninger, Principles of Biochemistry*. 6th ed. 2013: Worth Publishing.
25. Prabhu, A., et al., *Cysteine Catabolism: A Novel Metabolic Pathway Contributing to Glioblastoma Growth.* 2014. **74**(3): p. 787-796.
26. Lu, S.C., *Glutathione synthesis.* Biochimica et biophysica acta, 2013. **1830**(5): p. 3143-3153.
27. Balendiran, G.D., Rajesh; Fraser, Deborah, *The role of glutathione in cancer.* Cell Biochem Funct, 2004. **22**: p. 343-352.
28. Ogiwara, H., et al., *Targeting the Vulnerability of Glutathione Metabolism in ARID1A-Deficient Cancers.* Cancer Cell, 2019. **35**(2): p. 177-190.e8.
29. Mishra, P.A., Stefan;, *Metabolic Signatures of Human Breast Cancer.* Molecular and Cellular Oncology, 2015. **2**(3).
30. Lantermann, A.B., et al., *Inhibition of Casein Kinase 1 Alpha Prevents Acquired Drug Resistance to Erlotinib in EGFR-Mutant Non-Small Cell Lung Cancer.* Cancer Research, 2015. **75**(22): p. 4937-4948.
31. Kimbung, S., N. Loman, and I. Hedenfalk, *Clinical and molecular complexity of breast cancer metastases.* Seminars in Cancer Biology, 2015. **35**: p. 85-95.
32. Chiang, A.C. and J. Massague, *Molecular Origins of Cancer Molecular Basis of Metastasis.* New England Journal of Medicine, 2008. **359**(26): p. 2814-2823.
33. Carter, C.L., C. Allen, and D.E. Henson, *Relation of Tumor Size, Lymph-Node Status, and Survival in 24,740 Breast-Cancer Cases.* Cancer, 1989. **63**(1): p. 181-187.
34. Elston, C.W. and I.O. Ellis, *Pathological Prognostic Factors in Breast-Cancer .1. The Value of Histological Grade in Breast-Cancer - Experience from a Large Study with Long-Term Follow-Up.* Histopathology, 1991. **19**(5): p. 403-410.
35. Esserman, L.J., et al., *Biologic markers determine both the risk and the timing of recurrence in breast cancer.* Breast Cancer Research and Treatment, 2011. **129**(2): p. 607-616.
36. Gatza, M.L., et al., *Analysis of tumor environmental response and oncogenic pathway activation identifies distinct basal and luminal features in HER2-related breast tumor subtypes.* Breast Cancer Research, 2011. **13**(3).

37. Koppula, P., et al., *Amino acid transporter SLC7A11/xCT at the crossroads of regulating redox homeostasis and nutrient dependency of cancer.* Cancer Communications, 2018. **38**.
38. Eyupoglu, I.Y. and N.E. Savaskan, *Epigenetics in Brain Tumors: HDACs Take Center Stage.* Current Neuropharmacology, 2016. **14**(1): p. 48-54.
39. Aldana-Masangkay, G.I. and K.M. Sakamoto, *The Role of HDAC6 in Cancer.* Journal of Biomedicine and Biotechnology, 2011.
40. Angus, S.P., J.S. Zawistowski, and G.L. Johnson, *Epigenetic Mechanisms Regulating Adaptive Responses to Targeted Kinase Inhibitors in Cancer.* Annual Review of Pharmacology and Toxicology, Vol 58, 2018. **58**: p. 209-229.
41. Kim, K.H. and C.W.M. Roberts, *Targeting EZH2 in cancer.* Nature medicine, 2016. **22**(2): p. 128-134.
42. Eckschlager, T., et al., *Histone Deacetylase Inhibitors as Anticancer Drugs.* International Journal of Molecular Sciences, 2017. **18**(7).
43. Schlecht, N.F., et al., *Epigenetic changes in the CDKN2A locus are associated with differential expression of P16INK4A and P14ARF in HPV-positive oropharyngeal squamous cell carcinoma.* Cancer Medicine, 2015. **4**(3): p. 342-353.
44. Stott, F.J., et al., *The alternative product from the human CDKN2A locus, p14(ARF), participates in a regulatory feedback loop with p53 and MDM2.* Embo Journal, 1998. **17**(17): p. 5001-5014.
45. Romagosa, C., et al., *p16Ink4a overexpression in cancer: a tumor suppressor gene associated with senescence and high-grade tumors.* Oncogene, 2011. **30**: p. 2087.
46. Zhang, W. and J. Xu, *DNA methyltransferases and their roles in tumorigenesis.* Biomarker Research, 2017. **5**.
47. Luo, Y.H., et al., *UCH-L1 promotes invasion of breast cancer cells through activating Akt signaling pathway.* Journal of Cellular Biochemistry, 2018. **119**(1): p. 691-700.